Lead and slant on the geometry of coiling in gastropods

Ido Filin [1] *

[1] Independent researcher.

* Corresponding author. E-mail: ido@filin.fi

Running headline: Geometry of coiling.

Supplementary material: SI appendix.

The author(s) declare(s) no conflict of interest.

This manuscript was compiled on 28 May 2026.

Abstract

Molluscan shells have been studied with various geometric models. Here I show that *lead angle*, the defining slope of a conical helix, emerges as a more useful parameter in morphometric analyses and (adaptationist) interpretation of covariation in coiling parameters. The widely used apical semiangle becomes redundant and uninformative, a passive consequence of taxon-specific lead angles and plasticity in growth (expansion rate). Treating coiled shells as conical helices, and extending to *logarithmic slant helices* (curves of precession), provides insights into ontogenetic allometry, irregular coiling, past models, and unifying fixed- and moving-frame approaches.

Keywords: allometry, conchology, developmental plasticity, logarithmic spiral, malacology, ontogeny, slant helix, theoretical morphology

Letter

The equiangular, or logarithmic, spiral has a long and distinguished history, going back to Descartes, Torricelli, Christopher Wren, Newton, Halley, and the Bernoullis (Thompson [1942] 1992; Archibald 1918; Hammer 2016). Its application in biology, however, only picked up with Canon Henry Moseley and Carl Friedrich Naumann around 1840, who applied it to the study of molluscan shells, coinciding with the rapid development of paleontology in the 19th century (Moseley 1838, 1842; Naumann 1845; Thompson [1942] 1992; Raup 1966; Savazzi 1995; Vinarski 2014). Much of this earlier work on modeling and measurement of shells is thoroughly and eloquently summarized in D'Arcy Thompson's *magnum opus* "On Growth and Form" (Thompson [1942] 1992).

In "The geometry of coiling in gastropods", Raup (1961) sketched an earlier version of his parameter set for coiled geometries, that would later develop into theoretical morphology and the morphospace concept (Raup & Michelson 1965; Raup 1966, 1967; McGhee 1999; Pappas & Miller 2013; Gerber 2017). Essentially, though, Raup's model is a reformulation of the original *conispiral* parametrization of Moseley (1838) and Thompson ([1942] 1992) — a logarithmic spiral wrapped around a cone of *apical semiangle*, β, rather than winding on a plane (planispiral coiling, $\beta \to \pi/2$; Fig. 1A,D). Its defining feature is a fixed *spiral angle*, α, between the tangent of the spiral and its pole (or apex of the cone; hence, equiangular; Fig. 1A).

Conical logspirals also arise from fixed standardized *curvature* and *torsion* in the *differential geometric* formulation of Okamoto (1988), a local (moving) frame analysis (Fig. 1B) that he named the 'growing tube' model. A third alternative parameterization views the conical logspiral as a *conical helix* (Fig. 1C). The defining feature of a helix (more accurately, general or generalized helix, or curve of constant slope; Nutbourne & Martin 1988; Scofield 1995; SI) is the constant angle its tangent makes with some fixed direction. This direction determines the coiling axis, and the constant slope will be measured in this study by the downward angle of the coil, or helical thread, termed *lead angle*, λ in Fig. 1D. (Preserving here the distinction between 'pitch' and 'lead', in case of multi-thread helical structures, i.e., double or triple helices, or multi-start screws; see SI for more on terminology). If the coils wrap around a cone ($0 < \beta < \pi/2$), rather than a cylinder ($\beta \to 0$; the familiar circular helices of springs and corkscrews), such a conical helix is also a logarithmic conispiral. I dub this third parameterization *conihelical*. (Not to be confused with the 'helicocone' [Cox 1960] — the expanding tube itself, which usually coils around an axis to form the spiral shell.)

In the words of D'Arcy Thompson, "It seems a complicated affair; but it is only a pathway winding at a steady slope up a conical hill ... a certain ensemble, or bunch, of these spiral curves in space constitutes the self-similar surface of the shell" (Thompson [1942] 1992). In this letter, I explore how conical helices and their "steady slope", or lead angle, have underappreciated implications to morphometrics, interpretations of covariation in coiling parameters, and unifying *fixed-* and *moving-frame* approaches to theoretical morphology. In addition, conical helices can be extended to *slant helices*, particularly the *logarithmic slant helix* that I present here, to gain better understanding of ontogenetic allometry, irregular coiling, and previously formulated models of allometric spiral shells.

As hinted in the above quote, a shell is not a single conispiral, but a three-dimensional structure made of "a bunch" of such spirals — the *multispiral* approach (Fig. 1E; also called multivector; Thompson [1942] 1992; Bayer 1978; McGhee 1978, 1999; Savazzi 1990). Alternatively, a shell can be described by a *generating curve*, a closed figure that sweeps through space along a spiral *centerline* (Fig. 1F; Thompson [1942] 1992; Raup 1961, 1966; Okamoto 1988; equivalent, or roughly corresponding, to the 'center line locus' of Illert 1983, 'aperture trajectory' of Stone 1995, 'curve-skeleton' of Monnet *et al.* 2009, 'ontogeny axis' of Liew & Schilthuizen 2016, or 'internal spiral' of Larsson *et al.* 2020).

It is important to note that one can define the generating curve, and corresponding aperture sizes and aperture shape, either in the plane normal to the centerline tangent (as illustrated in Fig. 1F; Okamoto 1988; Monnet *et al.* 2009; 'orthoclinal' *sensu* Illert 1989; the $\hat{\mathbf{n}}$-$\hat{\mathbf{b}}$ plane, perpendicular to $\hat{\mathbf{t}}$ in Fig. 1A,B), or as a whorl cross-section in the (sagittal) plane containing the coiling axis (the z-r plane in Fig. 1D). The latter being the original formulation by Moseley (1838), Thompson ([1942] 1992) and Raup (1966). Aperture sizes in this cross-section plane will be denoted by a and b, respectively in radial (r) and axial (z) directions. Roughly corresponding aperture sizes in the normal plane are illustrated in Fig. 1F, denoted a^* and b^*. I conform here to much literature on morphospaces and shell morphometry, and refer henceforth to cross-section sizes, a and b, as aperture size, and to aperture shape as their ratio, $\rho = b/a$ (Raup 1966; Kohn & Riggs 1975; Ekaratne & Crisp 1983; Gerber 2017 ; but see SI).

In self-similar isometrically growing conihelical shells, the different spirals that make up the shell's surface, by geometric necessity, differ in spiral angle, α, apical semiangle, β, and lead angle, λ (Fig. 1E). However, they all share a single common value of exponential *expansion rate*, γ, with respect to revolution angle, θ (Illert 1983). Given linear measures of shell size, such as aperture size, a and b, centerline radius and height, r and z (Fig. 1D), or centerline

arclength, s, measured from the pole (or conical apex), one can define separate expansion parameters for each. However, for self-similar conihelical shells, these expansion rates are all equal, $\gamma_s = \gamma_a = \gamma_b = \gamma_z = \gamma_r = \gamma$. Alternatively, growth and size can be measured w.r.t arclength, s, rather than revolution angle, θ. For example, the relations $a(s)$ and $b(s)$, for aperture size, introduce Ackerly's (1989a) *dilation* parameter, which I denote here by $q_a = \mathrm{d}a/\mathrm{d}s$ and $q_b = \mathrm{d}b/\mathrm{d}s$. In isometric conihelical shells, q_a and q_b are constants, representing the opening angles of the expanding 'trumpet' or (helico)cone (Ekaratne & Crisp 1983; Ackerly 1989*a*; Vermeij 1993, 2002) that is coiled upon itself to make the spiral shell. Dilation factors for centerline r and z are just $q_r = \cos\alpha \sin\beta$ and $q_z = \sin\lambda = \cos\alpha \cos\beta$.

A set of formulas relates the conispiral, conihelical, and differential geometric parameterizations to each other and to expansion rates. One such formula is the aforementioned expression for q_z, relating lead angle, λ, to spiral angle, α. For expansion rate,

$$\cot\alpha \sin\beta = \gamma \tag{1}$$

(Moseley 1842; Thompson [1942] 1992; Raup & Graus 1972; Løvtrup & von Sydow 1974; Ekaratne & Crisp 1983; Illert 1983). Gastropod shells usually exhibit several complete whorls. Consequently, expansion rate is typically small, $\gamma \leq 0.2$ (Thompson [1942] 1992; Cameron 1981), leading to a similar, approximate, expression for the conihelical parameterization,

$$\tan\lambda \tan\beta \approx \gamma \tag{2}$$

(the exact expression being $\tan\lambda \tan\beta = \gamma/\sqrt{1+\gamma^2}$; see SI on approximation errors), demonstrating the three-way covariation of expansion rate, apical semiangle and lead angle.

Many empirical studies of shell coiling, in the past 50 years, have provided estimates of Raup's T and W parameters; or in terms of this study, $\tan\beta = 1/T$ and $\gamma = \ln W/2\pi$ respectively. Covariation of $\tan\beta$ and γ may point to adaptation, such as for mechanical strength, postural stability or economical shell construction (Raup 1966; Noshita *et al.* 2012; Okabe & Yoshimura 2017; Páll-Gergely *et al.* 2024), and is usually interpreted through Raup's (1966) condition for tight coiling, or whorl overlap, $\tan\beta > \sinh(\pi\gamma)$, given circular apertures (SI). (Alternatively, $\sin\beta > \tanh(\pi\gamma)$; corresponding to the expression by Clarke *et al.* 1999, accounting for the typo in their equation, and the difference in definition of apical angle; SI). However, for small γ, typical of most gastropods, the whorl overlap boundary is practically indistinguishable from the seemingly arbitrary condition $\lambda < \arctan(1/\pi)$ (0.318 or 17.66°; Fig. 2A; SI). Similar conditions can be formulated for non-circular apertures (SI). A geometric constraint on lead

(or spiral) angle, combined with variation in growth rate (shell expansion), can therefore produce, given Eq.[2], the empirically observed direct relation between $\tan\beta$ and γ.

Past hints to the relative constancy of lead angles can also be glimpsed from observations of ontogenetic patterns, where measurements of $\tan\beta$ and γ at different whorls or developmental stages vary together, so to preserve an almost fixed ratio (e.g., Davoli & Russo 1974; Newkirk & Doyle 1975; Hutchinson 1989; Clarke *et al.* 1999). In particular, Ekaratne & Crisp's (1983) shell-height-to-arclength ratio contains a $1/\sec\alpha\sec\beta$ factor, which is just $q_z = \sin\lambda$ of this study. In fact, their formula can be rewritten as $H/s = z/s + b/s = q_z + q_b = \sin\lambda + q_b$ (SI). Lead angle, therefore, a defining feature of conical helices, emerges as a more useful parameter for interpreting morphometric (co)variation (Fig. 2B). Variation in apical semiangle (β; Fig. 2A) follows as a passive consequence of growth (variation in γ) and geometry (lead angle, λ) of the expanding centerline spiral (Eq.[2]).

Lead angle, however, is expected to vary ontogenetically to some degree. For example, Savazzi (1990) discussed deviated protoconchs (see also Cox 1960; Frýda & Ferrová 2011); van Osselaer & Grosjean (2000) fitted conispirals piecewise to several species, and showed three ontogenetic phases — protoconch, and early and late conispiral phases — with different coiling parameters (see also Davoli & Russo 1974); and Newkirk & Doyle (1975) reported values of coiling parameters for embryos and adults in a study of geographic variation in the rough periwinkle, *Littorina saxatilis* (Fig. 2).

Variation in lead angle can be further understood by considering the differential geometric parameterization. In helices, coiling angle per unit of centerline arclength, $\mathrm{d}\theta/\mathrm{d}s$, is measured by the norm of the *Darboux vector*, $\mathbf{u} = u\hat{\mathbf{u}}$, the instantaneous rotation vector of the Frenet frame along its defining space curve (Fig. 1B; Chouaieb *et al.* 2006; Goriely 2017). In generalized helices, $\hat{\mathbf{u}}$ coincides with the fixed coiling axis. The norm of the Darboux vector, $\|\mathbf{u}\| = u$, is the 'compound curvature' of Nutbourne & Martin (1988), the 'first alternative curvature' of Güzelkardeşler & Şahiner (2024), and the familiar $\sqrt{\kappa^2+\tau^2}$ of differential geometric literature (also D_G and A_G of Noshita 2014 and Noshita *et al.* 2016, who used Okamoto's growing tube formulation; clearly related in their experssions to angular rate, $\mathrm{d}\theta/\mathrm{d}s$). In this letter, I refer to u as *local coiling*. The constant lead angle of general helices is determined by the torsion-curvature ratio, $\tan\lambda = \tau/\kappa$, $\kappa = u\cos\lambda$, and $\tau = u\sin\lambda$.

Conical helices are further defined by local coiling that is inversely proportional to arclength (Nutbourne & Martin 1988). We can therefore write $u = \tilde{u}/s$, where $\tilde{u}$ is constant dimensionless *standardized local coiling* (though the 'standardization' here is different than Okamoto's).

Arclength expansion rate, γ_s, is then related to (standardized) local coiling by the simple and intuitive relation $\gamma_s = 1/\tilde{u}$ (SI). As local coiling and curvature increase, the conical helix coils tighter, and less arclength growth and radial expansion is gained per full revolution. Hence, more whorls are required for a specified amount of (relative) growth. This helps to explain the association of high-spired species with large numbers of whorls (Cain 1980) and Gould's so-called "jigsaw constraint", originally observed in his study of *Cerion* (Gould 1989; Béguinot 2021).

Allometric modifications of conical helices, such as the logarithmic *helicospiral* model, derived many times in various guises (essentially, $\gamma_z \neq \gamma_r$; Kohn & Riggs 1975; Bayer 1978; Cortie 1989; Schindel 1990; Savazzi 1990; Fowler *et al.* 1992; Stone 1995; Tursch 1997; van Osselaer & Grosjean 2000; Urdy *et al.* 2010; Swan 2015; Larsson *et al.* 2020), and Harary & Tal's (2011) 'natural 3D spiral' do not have constant lead angles, and are therefore not generalized helices. Rate of change in lead angle, $\lambda' = \mathrm{d}\lambda/\mathrm{d}s$, is equivalent to the 'second alternative curvature' of Uzunoğlu *et al.* (2016) and Güzelkardeşler & Şahiner (2024) (see SI). If $\lambda' \neq 0$, the Darboux vector of local coiling and the fixed coiling axis of the helicospiral do not coincide, as the former now rotates around the latter (Fig. 1G). This new rotation axis is

$$\begin{aligned} \mathbf{w} &= w\hat{\mathbf{w}} = \mathbf{u} + \lambda'\hat{\mathbf{n}} = u\hat{\mathbf{u}} + \lambda'\hat{\mathbf{n}}, \\ w &= \|\mathbf{w}\| = \sqrt{u^2 + (\lambda')^2} = \sqrt{\kappa^2 + \tau^2 + (\lambda')^2}, \end{aligned} \tag{3}$$

dubbed here respectively vector and rate of *total coiling*. This full coiling rate (and direction) contains both a local coiling component, u, and a λ' component (first and second 'alternative curvatures' of Uzunoğlu *et al.* 2016 and Güzelkardeşler & Şahiner 2024; generalized helices are obtained when $\lambda' = 0$). The latter can be referred to as *coiling precession* rate, further explained at the end of this letter.

Four decades ago, Løvtrup & Løvtrup (1988) attempted to "move the β parameter down to the mantle edge". In other words, derive a parameter of global shell shape from local processes occurring at the aperture. Løvtrup & Løvtrup's partial solution was to replace β with the ratio of maximum and minimum growth rates around the aperture. An explanation that Hutchinson (1990) debunked shortly after. Through Eqs.[1] and [2], however, the apical semiangle can indeed be "eliminated", or "moved down" to the aperture, as γ, α, and λ are defined at the growing tip (i.e., tangent) of conispirals, or conical helices. The distinction between fixed- (conispiral and conihelical) and moving-frame (differential geometric) parameterizations, thus, begins to blur.

Another defining feature of fixed-frame models is, for obvious reasons, the fixed coiling

axis. Rate of change in the direction of local coiling, $\hat{\mathbf{u}}$, is given by $\hat{\mathbf{u}}' = \mathbf{w} \times \hat{\mathbf{u}} = u\hat{\mathbf{u}} \times \hat{\mathbf{u}} + \lambda'\hat{\mathbf{n}} \times \hat{\mathbf{u}} = \lambda'\hat{\mathbf{n}} \times \hat{\mathbf{u}}$. In conihelical shells ($\lambda' = 0$), the Darboux vector, $\mathbf{u}$, defines the fixed coiling axis. Thus, given starting coiling direction (initial condition), conispiral coiling can be defined by apical and spiral angles, by lead angle and expansion rate, by lead angle and standardized local coiling, $\tilde{u}$, or by Okamoto's standardized curvature and torsion. In all four cases, if parameter values remain fixed, the initial coiling direction is maintained ($\hat{\mathbf{u}}' = 0$), becoming a fixed axis, and self-similar conispiral shells result. That is another metric by which the distinction between fixed- and moving-frame parametrizations seems superfluous.

Irregular coiling, allometry, or other deviations from self-similar conihelical geometry, always require a change in parameter values (notably, lead angle). Gradual rotation of the local coiling axis, $\hat{\mathbf{u}}$, thus, occurs simultaneously with (transient) change in lead angle ($\lambda' \neq 0$), and by rotating around the vector of total coiling, $\mathbf{w}$ (Fig. 1G). That is, in fact, another direct consequence of conihelical geometry; this time, prescribing a testable hypothesis on how shell geometry can deviate from isometric conihelical. Some evidence in support of this hypothesis appears in Ackerly's (1989*b*) visual and stereographic analyses of *Vermicularia*, which possesses a tightly coiled conispiral juvenile phase, followed by an open-coiled geometry that differs in both coiling axis and lead angle. Similarly, his analysis of *Distorsio* shows that lead angle varies among successive episodic growth increments, while the per-increment coiling axis wobbles with an angular radius of roughly four to seven degrees. Savazzi (1996) provides examples from several species of *Tenagodus* (syn. *Siliquaria*) and *Vermicularia* that follow the same rule of simultaneous change in coiling axis and in lead angle. Particularly extreme cases occur in microsnails (Clements *et al.* 2008; Liew *et al.* 2014) and in irregularly coiled (heteromorph) ammonoids (Okamoto 1988, 1996).

Initially, the allometric logarithmic helicospiral ($\gamma_z \neq \gamma_r$) seems to contradict the hypothesis, as lead angle increases ($\gamma_z > \gamma_r$) or decreases ($\gamma_z < \gamma_r$), while the coiling axis remains fixed. Similarly, in Harary & Tal's (2011) 'natural 3D spiral', lead angle varies smoothly between a starting value, λ_0, and an asymptotic value, λ_∞, at large arclengths; essentially, converging to a conispiral (though adult size and shape may be obtained well before that asymptote is reached). However, when the direction of $\mathbf{w} = u\hat{\mathbf{u}} + \lambda'\hat{\mathbf{n}}$ does not change, it acts as the new fixed coiling axis of the shell; its magnitude, $w = \sqrt{u^2 + (\lambda')^2}$, is the coiling rate around that axis (i.e., revolution angle per unit growth of centerline arclength, $\mathrm{d}\theta/\mathrm{d}s = w = \|\mathbf{w}\|$). This rotation of the local moving Frenet frame around a potentially fixed axis, $\hat{\mathbf{w}}$, is another reason why fixed- and moving-frame models should be considered in tandem, as complementary points of view.

The condition of fixed $\hat{\mathbf{w}}$ is satisfied, for example, when local coiling and change in lead angle are both constant, $u = \text{const}$, $\lambda' = \text{const}$. These are the 'modulated curves' of Nutbourne & Martin (1988), better known as 'curves of constant precession' (Scofield 1995). Another class of curves, in which $\hat{\mathbf{w}}$ is fixed, are the already familiar conical and generalized helices. This is just the degenerate case of $\mathbf{w} = \mathbf{u}$ and $\lambda' = 0$, where the precession vanishes. Extrapolating from both curves of constant precession and curves of constant slope (generalized helices), one obtains a class of curves called *slant helices* that includes the former two as special cases. A necessary and sufficient condition for a slant helix, in the notation of this study, is $\lambda' \propto u$, or $\lambda' = \sigma u$ where $\sigma = \text{const}$ (Izumiya & Takeuchi 2004 ; SI).

We can proceed still one step further and define the *logarithmic slant helix*, $u, \lambda' \propto 1/s$, or $u = \tilde{u}/s$ and $\lambda' = \sigma\tilde{u}/s$, where σ and $\tilde{u}$ are constants (SI). While the logarithmic slant helix describes an allometrically growing shell, it does share some properties with the isometric conical helix. For example, revolution angle and arclength are similarly related through $\theta \propto \ln(s/s_0)$, and therefore arclength expands exponentially, $s = s_0 e^{\gamma_s \theta}$, where $\gamma_s = 1/\tilde{w}$, $\tilde{w} = \tilde{u}\sqrt{1+\sigma^2}$. Another feature of logarithmic slant helices is that lead angle grows linearly with θ. Successive whorls, separated by a full revolution around the coiling axis ($\Delta\theta = 2\pi$), are always tilted relative to each other by the same amount, $\Delta\lambda = 2\pi\lambda'/w = 2\pi\sigma/\sqrt{1+\sigma^2}$ (Fig. 1H). (This last result is roughly reminiscent of angular increments in Hutchinson's [1989] 'road-holding' model.)

The logarithmic slant helix, thus, is a natural allometric extension of the isometric conical helix, in the sense that, instead of being fixed on the same initial value (λ_0) throughout ontogeny, lead angle grows linearly (i.e., $\lambda(\theta) = \lambda_0 + c\theta$; $c = \text{const}$). In that respect, it is the simplest case of centerline allometry, and provides insight into other allometric models (helicospirals, $\gamma_z \neq \gamma_r$, or Harary & Tal 2011). Lead angle cannot grow indefinitely, unless coiling becomes open and irregular. But real shells have a finite number of whorls, and therefore, the logarithmic slant helix, like its older cousin, the conical helix, is a useful approximation. In particular, given expressions for the centerline curve, $x(\theta)$, $y(\theta)$, and $z(\theta)$ (SI), one can simulate such shells graphically (Fig. 1H,I).

Finally, Illert (1983, 1987, 1989) envisioned the coiled shell as a spiral clock spring (see also, Illert & Santilli 1995; Savazzi 1995; McGhee 1999). In light of this letter, rather than a clock spring, the coiled shell may be viewed as a precessing gyroscope, or spinning top. In the moving and rotating Frenet frame, the total coiling vector, $\mathbf{w}$, analogous to the spin of the gyroscope, precesses around the $\hat{\mathbf{n}}$ direction at a rate λ'; resulting in an "interchange between

curvature and torsion" (Nutbourne & Martin 1988), respectively the $\hat{\mathbf{b}}$- and $\hat{\mathbf{t}}$-components of $\mathbf{w}$. The constant σ determines the tilt angle, just as a precessing gyroscope is tilted relative to the horizontal plane, with the tilt determining the rate of precession (here, $\lambda' \propto \sigma$). With this Kirchhoff-kinetic-analogy-like argument (Nizette & Goriely 1999), we gain yet another viewpoint whereby moving- and fixed-frame modeling are complementary.

Supplementary information

Additonal derivations, explanations, methods, and discussion are in the supplementary information document.

DATA AND SOFTWARE AVAILABILITY. All data and code are available at https://doi.org/10.5281/zenodo.19763620, for the data analyses (Fig. 2), and at https://doi.org/10.5281/zenodo.19895626, for the `WebGL` application of theoretical morphology of coiled shells (Fig. 1).

References

Ackerly SC (1989*a*). Kinematics of accretionary shell growth, with examples from brachiopods and molluscs. *Paleobiology* 15: 147–164. 10.1017/s0094837300009337.

Ackerly SC (1989*b*). Shell coiling in gastropods; analysis by stereographic projection. *PALAIOS* 4: 374–378. https://doi.org/10.2307/3514561.

Araki A, Noshita K (2023). Theoretical morphological analysis of differential morphospace occupation patterns for terrestrial and aquatic gastropods. *Evolution* 77: 1864–1873. https://doi.org/10.1093/evolut/qpad110.

Archibald RC (1918). The logarithmic spiral (undergraduate mathematics clubs, topics for club programs). *American Mathematical Monthly* 25: 189–193.

Bayer U (1978). Morphogenetic programs, instabilities, and evolution — a theoretical study. *Neues Jahrb Geol Paläont Abh* 156: 226–261. 10.1127/njgpa/156/1978/226.

Béguinot J (2021). Adult shell-size regulation in conispirally-coiled shells: evidence for a widespread negative covariance between whorls growth-rate and the final number of whorls in land snails. *Annual Research & Review in Biology* 36: 95–106. https://doi.org/10.9734/arrb/2021/v36i1030439.

Cain AJ (1980). Whorl number, shape, and size of shell in some pulmonate faunas. *J Conchol* 30: 209–221.

Cameron RAD (1981). Functional aspects of shell geometry in some british land snails. *Biol J Linn Soc* 16: 157–167. https://doi.org/10.1111/j.1095-8312.1981.tb01648.x.

Chouaieb N, Goriely A, Maddocks JH (2006). Helices. *Proc Natl Acad Sci USA* 103: 9398–9403. https://doi.org/10.1073/pnas.0508370103.

Clarke RK, Grahame J, Mill PJ (1999). Variation and constraint in the shells of two sibling species of intertidal rough periwinkles (Gastropoda: *Littorina* spp.). *J Zool* 247: 145–154.

10.1111/j.1469-7998.1999.tb00978.x.

Clements R, Liew TS, Vermeulen JJ, Schilthuizen M (2008). Further twists in gastropod shell evolution. *Biology Letters* 4: 179 – 182. https://doi.org/10.1098/rsbl.2007.0602.

Cortie M (1989). Models for mollusc shell shape. *South African Journal of Science* 85: 454–460.

Cox LR (1960). Gastropoda. General characteristics of Gastropoda. In *Treatise on Invertebrate Paleontology*, Part I, pp. I84–I169. Geological Society of America and University of Kansas Press, New York, NY and Lawrence, KS.

Davoli F, Russo F (1974). Una metodologia paleontometrica basata sul modello di Raup: verifica sperimentale su rappresentanti fossili del gen. *Subula* Schumacher. *Bollettino della Società Paleontologica Italiana* 13: 108–121. https://www.paleoitalia.it/wp-content/uploads/2023/04/5-Davoli-Russo.pdf.

Ekaratne SUK, Crisp DJ (1983). A geometric analysis of growth in gastropod shells, with particular reference to turbinate forms. *Journal of Marine Biology Association UK* 63: 777–797. 10.1017/S0025315400071216.

Fowler DR, Meinhardt H, Prusinkiewicz P (1992). Modeling seashells. *Proceedings of the 19th annual conference on Computer graphics and interactive techniques*, pp. 379–387. 10.1145/133994.134096.

Frýda J, Ferrová L (2011). The oldest evidence of non-coaxial shell heterostrophy in the class Gastropoda. *Bull Geosci* 86: 765–776. 10.3140/bull.geosci.1302.

Gerber S (2017). The geometry of morphospaces: lessons from the classic Raup shell coiling model. *Biol Rev* 92: 1142–1155. https://doi.org/10.1111/brv.12276.

Goriely A (2017). *The Mathematics and Mechanics of Biological Growth*. Springer. https://doi.org/10.1007/978-0-387-87710-5.

Gould SJ (1989). A developmental constraint in *Cerion*, with comments on the definition and interpretation of constraint in evolution. *Evolution* 43: 516–539. 10.1111/j.1558-5646.1989.tb04249.x.

Güzelkardeşler G, Şahiner B (2024). An alternative approach to find the position vector of a general helix. *Celal Bayar University Journal of Science* 20: 54–60. 10.18466/cbayarfbe.1479066.

Hammer Ø (2016). *Perfect Shape: Spiral Stories*. Springer.

Harary G, Tal A (2011). The natural 3D spiral. *Computer Graphics Forum* 30: 237–246. https://doi.org/10.1111/j.1467-8659.2011.01855.x.

Hutchinson JMC (1989). Control of gastropod shell shape: the role of the preceding whorl. *J Theor*

Biol 140: 431–444. 10.1016/S0022-5193(89)80107-9.

Hutchinson JMC (1990). Control of gastropod shell form via aperture growth rates. *J Morphol* 206: 259–264. 10.1002/jmor.1052060302.

Illert C (1983). The mathematics of gnomonic seashells. *Math Biosci* 63: 21–56. 10.1016/0025-5564(83)90049-4.

Illert C (1987). Formulation and solution of the classical seashell problem. I. - Seashell geometry. *Il Nuovo Cimento D* 9: 791–814. 10.1007/BF02453750.

Illert C (1989). Formulation and solution of the classical seashell problem. II. - Tubular three-dimensional seashell surfaces. *Il Nuovo Cimento D* 11: 761–780. 10.1007/BF02451562.

Illert CR, Santilli RM (1995). *Foundations of Theoretical Conchology: From Self-Similarity in Non-Conservative Mechanics*. 2nd edn. Hadronic Press, Palm Harbor, FL. OCLC: 34320294.

Izumiya S, Takeuchi N (2004). New special curves and developable surfaces. *Turkish Journal of Mathematics* 28: 153–164. 10.14943/83700.

Kohn AJ, Riggs AC (1975). Morphometry of the *Conus* shell. *Syst Zool* 24: 346–359. 10.1093/sysbio/24.3.346.

Larsson J, Westram AM, Bengmark S, Lundh T, Butlin RK, Butlin RK (2020). A developmentally descriptive method for quantifying shape in gastropod shells. *J R Soc Interface* 17. http://dx.doi.org/10.1098/rsif.2019.0721.

Liew TS, Kok ACM, Schilthuizen M, Urdy S (2014). On growth and form of irregular coiled-shell of a terrestrial snail: *Plectostoma concinnum* (Fulton, 1901) (Mollusca: Caenogastropoda: Diplommatinidae). *PeerJ* 2: e383. https://doi.org/10.7717/peerj.383.

Liew TS, Schilthuizen M (2016). A method for quantifying, visualising, and analysing gastropod shell form. *PLOS ONE* 11: 1–24. https://doi.org/10.1371/journal.pone.0157069.

Løvtrup S, Løvtrup M (1988). The morphogenesis of molluscan shells: a mathematical account using biological parameters. *J Morphol* 197: 53–62. 10.1002/jmor.1051970105.

Løvtrup S, von Sydow B (1974). D'Arcy Thompson's theorem and the shape of the molluscan shell. *Bull Math Biol* 36: 567–575. 10.1016/S0092-8240(74)80051-0.

McGhee GR (1978). Analysis of the shell torsion phenomenon in the Bivalvia. *Lethaia* 11: 315–329. https://doi.org/10.1111/j.1502-3931.1978.tb01889.x.

McGhee GR (1999). *Theoretical Morphology : The Concept and Its Applications*. Perspectives in Earth History and Paleobiology. Columbia University Press, New York.

Monnet C, Zollikofer C, Bucher H, Goudemand N (2009). Three-dimensional morphometric ontogeny of mollusc shells by micro-computed tomography and geometric analysis. *Palaeontol Electron* 12: 1–13. https://doi.org/10.5167/uzh-23587.

Moseley H (1838). XVII. On the geometrical forms of turbinated and discoid shells. *Phil Trans R Soc* 128: 351–370. https://doi.org/10.1098/rstl.1838.0018.

Moseley H (1842). On conchyliometry. *Lond Edinb Dubl Phil Mag* 21: 300–305. https://doi.org/10.1080/14786444208621551.

Naumann CF (1845). Über die wahre Spirale der Ammoniten. *Annalen der Physik* 140: 538–543. https://doi.org/10.1002/andp.18451400406.

Newkirk GF, Doyle RW (1975). Genetic analysis of shell-shape variation in *Littorina saxatilis* on an environmental cline. *Mar Biol* 30: 227–237. 10.1007/BF00390745.

Nizette M, Goriely A (1999). Towards a classification of euler–kirchhoff filaments. *Journal of Mathematical Physics* 40: 2830–2866. https://doi.org/10.1063/1.532731.

Noshita K (2014). Quantification and geometric analysis of coiling patterns in gastropod shells based on 3D and 2D image data. *J Theor Biol* 363: 93–104. 10.1016/j.jtbi.2014.08.010.

Noshita K, Asami T, Ubukata T (2012). Functional constraints on coiling geometry and aperture inclination in gastropods. *Paleobiology* 38: 322–334. 10.1666/10060.1.

Noshita K, Shimizu K, Sasaki T (2016). Geometric analysis and estimation of the growth rate gradient on gastropod shells. *J Theor Biol* 389: 11–19. 10.1016/j.jtbi.2015.10.011.

Nutbourne AW, Martin RR (1988). *Differential geometry applied to curve and surface design: Foundations*. Ellis Horwood, Chichester, England.

Okabe T, Yoshimura J (2017). Optimal designs of mollusk shells from bivalves to snails. *Scientific Reports* 7: 42445. https://doi.org/10.1038/srep42445.

Okamoto T (1988). Analysis of heteromorph ammonoids by differential geometry. *Paleobiology* 31: 35–52.

Okamoto T (1996). Theoretical modeling of ammonoid morphology. In *Ammonoid Paleobiology* (edited by Landman NH, Tanabe K, Davis RA), pp. 225–251. Springer US, Boston, MA. https://doi.org/10.1007/978-1-4757-9153-2_8.

Páll-Gergely B, Sipos AÁ, Harzhauser M, Örstan A, Winkler V, Neubauer TA (2024). Many roads to success: alternative routes to building an economic shell in land snails. *Evolution* 78: 778–786. https://doi.org/10.1093/evolut/qpae018.

Pappas JL, Miller DJ (2013). A generalized approach to the modeling and analysis of 3d surface morphology in organisms. *PLOS ONE* 8: 1–15. https://doi.org/10.1371/journal.pone.0077551.

Raup DM (1961). The geometry of coiling in gastropods. *Proc Natl Acad Sci USA* 47: 602–609. https://doi.org/10.1073/pnas.47.4.602.

Raup DM (1966). Geometric analysis of shell coiling: general problems. *J Paleontol* 40: 1178–1190.

Raup DM (1967). Geometric analysis of shell coiling: coiling in ammonoids. *J Paleontol* 41: 43–65.

Raup DM, Graus RR (1972). General equations for volume and surface area of a logarithmically coiled shell. *Mathematical Geology* 4: 307–316. 10.1007/BF02114092.

Raup DM, Michelson A (1965). Theoretical morphology of the coiled shell. *Science* 147: 1294–1295. 10.1126/science.147.3663.1294.

Savazzi E (1990). Biological aspects of theoretical shell morphology. *Lethaia* 23: 195–212. 10.1111/j.1502-3931.1990.tb01360.x.

Savazzi E (1995). Theoretical shell morphology as a tool in constructional morphology. *Neues Jahrb Geol Paläont Abh* 195: 229–240. 10.1127/njgpa/195/1995/229.

Savazzi E (1996). Adaptaions of vermetid and siliquarid gastropods. *Palaeontology* 39: 157–177.

Schindel DE (1990). Unoccupied morphospace and the coiled geometry of gastropods: architectural constraint or geometric covariation? In *Causes of Evolution: a paleontological perspective* (edited by Ross R, Allmon W), pp. 270–304. University of Chicago Press, Chicago.

Scofield PD (1995). Curves of constant precession. *The American Mathematical Monthly* 102: 531–537. https://doi.org/10.1080/00029890.1995.12004613.

Stone JR (1995). CerioShell: a computer program designed to simulate variation in shell form. *Paleobiology* 21: 509–519. 10.1017/S0094837300013518.

Swan ARH (2015). Heterochrony in helicoid spiral cones: a computer model for demonstrating heterochronic evolution. *Palaeontol Electron* 18: 1–11. 10.26879/510.

Thompson DW ([1942] 1992). *On Growth and Form: The Complete Revised Edition.* Dover, New York.

Tursch B (1997). Spiral growth: The 'Museum of all shells' revisited. *J Molluscan Stud* 63: 547–554. https://doi.org/10.1093/mollus/63.4.547.

Urdy S, Goudemand N, Bucher H, Chirat R (2010). Allometries and the morphogenesis of the molluscan shell: a quantitative and theoretical model. *J Exp Zool* 314B: 280–302. 10.1002/jez.b.21337.

Uzunoğlu B, Gök I, Yaylı Y (2016). A new approach on curves of constant precession. *Applied*

Mathematics and Computation 275: 317–323. https://doi.org/10.1016/j.amc.2015.11.083.

van Osselaer C, Grosjean P (2000). Suture and location of the coiling axis in gastropod shells. *Paleobiology* 26: 238–257. 10.1666/0094-8373(2000)026<0238:SALOTC>2.0.CO;2.

Vermeij GJ (1993). *A Natural History of Shells.* Princeton University Press, Princeton, Oxford.

Vermeij GJ (2002). Characters in context: molluscan shells and the forces that mold them. *Paleobiology* 28: 41–54. 10.1666/0094-8373(2002)028<0041:CICMSA>2.0.CO;2.

Vinarski MV (2014). The birth of malacology. when and how? *Zoosystematics and Evolution* 90: 1–5. 10.3897/zse.90.7008.

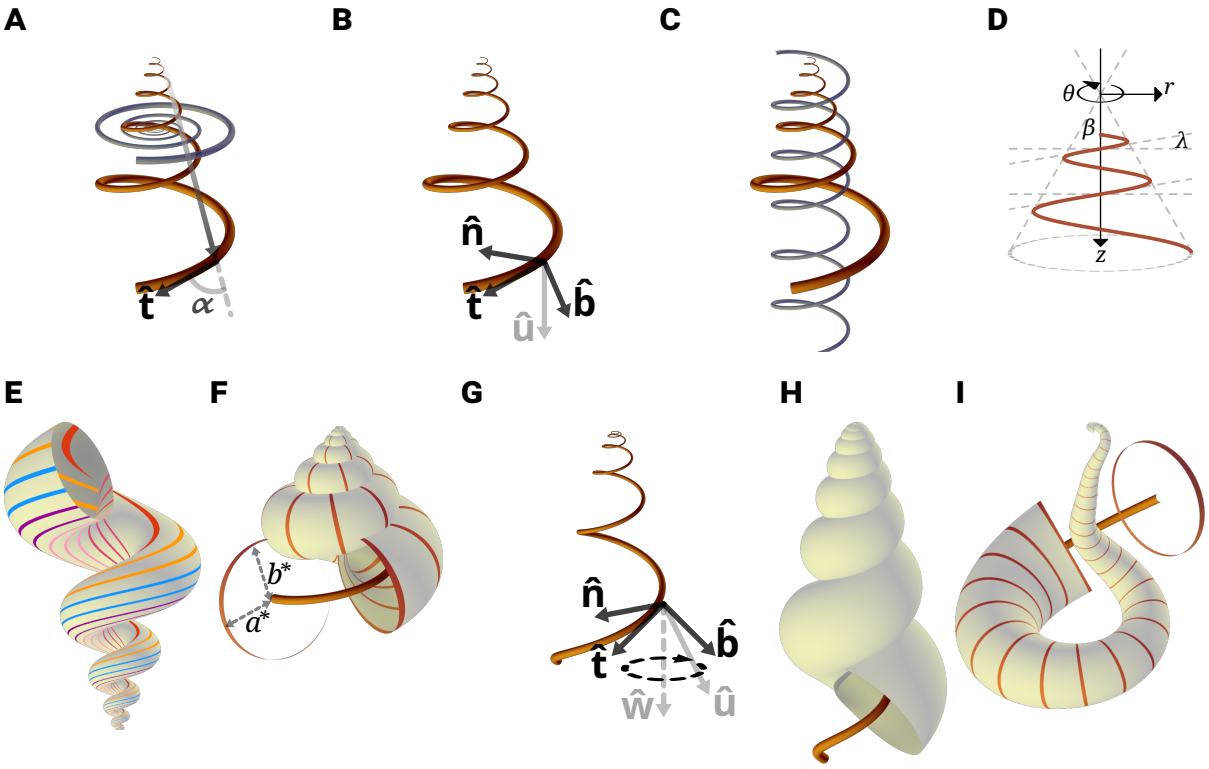

Figure 1 : Theoretical morphology in a snailshell. (***A,B,C***) Three parameterizations of conical logspirals; respectively conispiral, differential geometric, and conihelical. (***A***) Constant spiral angle, α, between instantaneous tangent vector, $\hat{\mathbf{t}}$, and radius-vector from pole (apex) defines the conispiral parameterization. The conispiral is as if a corresponding logarithmic base planispiral (in blue), with same expansion rate, γ, has been stretched out of its plane, to form a three-dimensional space curve. (***B***) The differential geometric parameterization follows the evolution of the Frenet moving frame, defined by tangent, $\hat{\mathbf{t}}$, principal normal, $\hat{\mathbf{n}}$, and binormal, $\hat{\mathbf{b}} = \hat{\mathbf{t}} \times \hat{\mathbf{n}}$. The frame's rotation is defined by the Darboux vector $\mathbf{u} = u\hat{\mathbf{u}} = \tau\hat{\mathbf{t}} + \kappa\hat{\mathbf{b}} = u\sin\lambda\hat{\mathbf{t}} + u\cos\lambda\hat{\mathbf{b}}$; κ is curvature, and τ torsion (SI). (***C***) In the conihelical parameterization, a conical logspiral is viewed as a helix with expanding radius — a conical helix. For comparison, a circular helix with same slope (i.e., lead angle) is also illustrated. (***D***) Conical helix in side view. Apical semiangle, β, lead angle, λ, and the cylindrical coordinate system illustrated. The z-direction coincides with the coiling axis. (***E***) Multispiral approach to shell modeling, where shell surface is defined by many spiral paths, differing in lead angle. For illustration purposes, an exaggerated open-coiled shell is shown, where slopes of inner spirals are clearly steeper. Nevertheless, all spirals share the same expansion rate, γ. (***F***) Generating curve approach to shell modeling. Shell surface defined by a closed figure (here a circle) that sweeps along a conihelical centerline. Also illustrated are the 'orthoclinal' (Illert 1987) of 'growing tube' (Okamoto 1988) aperture sizes, a^* and b^* (not to be confused with the binormal vector, $\hat{\mathbf{b}}$), roughly corresponding respectively to aperture size perpendicular and parallel to the coiling axis. (***G***) In allometric shells, where centerline lead angle varies, the Darboux vector is no longer fixed, but rotates around an axis $\mathbf{w} = w\hat{\mathbf{w}}$ that contains a λ' component (Eq.[3]; SI). (***H,I***) Allometric and irregularly coiled shells with logarithmic slant helix centerline. Lead angles are initially 0 (i.e., planispiral coiling), but subsequently grow at different rates. Parameter values to simulate all shell images of this figure in the `WebGL` application are provided in SI.

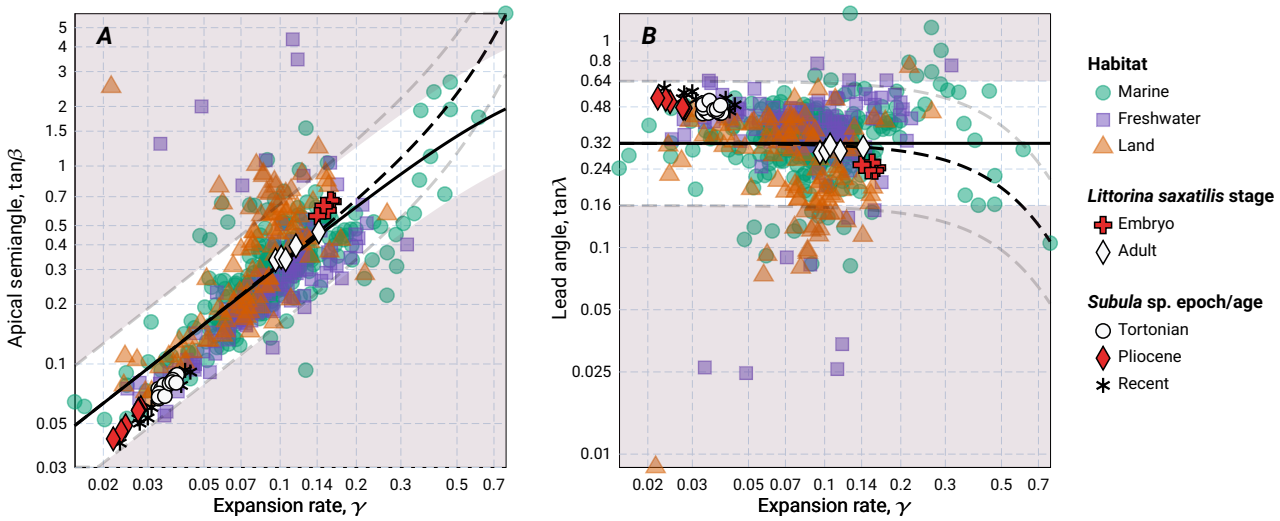

Figure 2 : Apical semiangle, as $\tan\beta$ (panel A), and lead angle, as $\tan\lambda$ (panel B), against expansion rate, $\gamma = \ln W/2\pi$, from the data in Noshita *et al.* (2012) and Araki & Noshita (2023) on coiling parameters of over 400 species of marine, freshwater, and terrestrial gastropods, the data of Newkirk & Doyle (1975) on embryos and adults of *Littorina saxatilis* from five different populations in Nova Scotia (scatter points represent population means), and the data of Davoli & Russo (1974) on high-spired *Subula* (syn. *Terebera*) from three different geological epochs (scatter points represent various subsample means, according to epoch/age, juvenile vs. adult whorls, and shell sculpture). In both panels, most data is in the region $\gamma \leq 0.2$, roughly the domain of validity for small-γ approximations (SI). All curves and shading, however, were drawn using full (non-approximate) expressions (SI). Additionally, for both panels, most data falls in the unshaded region, defined by fixed lead angles between 0.16 and 0.64 ($1/2\pi \leq \lambda \leq 2/\pi$), where the solid black line is $\lambda = 1/\pi = 0.32$. (***A***) When apical semiangle is plotted against expansion rate, a clear linear trend is visible. Dashed lines indicate boundaries for whorl-overlap, $\tan\beta > (1/\rho)\sinh(\pi\gamma)$, for $\rho = 0.5,\ 1,\ 2$ (upper to lower), that separates tightly-coiled from open-coiled shells (above and below boundary line respectively). ($\rho = b/a$; $\rho = 1$ represents circular generating curves — middle dashed line.) In the range $\gamma \leq 0.2$, such whorl-overlap boundaries, however, are practically indistinguishable from relationships that fixed lead angles in Eq.[2] prescribe ($\tan\beta = \left(\gamma/\sqrt{1+\gamma^2}\right)\cot\lambda$; solid black line and boundaries of shaded areas), given $\tan\lambda = \rho/\pi$ (SI; $D = 0$ for illustrated curves; i.e., apertures touching the coiling axis). Raw values for apical angles were transformed to correspond to centerlines by doubling reported values of T (as explained also in Davoli & Russo 1974). (***B***) Estimates of lead angle, $\tan\lambda$, obtained from the non-approximate version of Eq.[2]. Compared to panel A, there is clearly less variation in lead angle than in apical angle, and linear trends, in all datasets and groupings, disappear; suggesting independent variation (Gerber 2017) in expansion rate, γ, and lead angle, λ. Whorl-overlap curves correspond to those in panel A, but in reverse upper-to-lower order.

Supplementary information for “Lead and slant on the geometry of coiling in gastropods”

Ido Filin [1] *

[1] Independent researcher.

* Corresponding author. E-mail: ido@filin.fi

Contents

S1 A note on terminology and notation

Thompson ([1942] 1992) defined three angles, related to the modeling of equiangular (i.e., logarithmic) spiral shells. The spiral angle, α, is the angle between the radius-vector from the pole (or apex of the conical envelope) and the tangent to the spiral. His β denotes the apical semiangle, as in this study. His γ refers to the 'angle of retardation', relevant when considering the inner and outer margins of planispiral shells. Given that the angle of retardation has been rarely utilized since, I reclaim the symbol γ for denoting the exponential expansion rate in this study.

Generalized or general helices (Nutbourne & Martin 1988) are defined by the constant slope, relative to a fixed direction. Hence, the alternative term, curve of constant slope (Scofield 1995). Somewhat confusingly they are also often called 'cylindrical helices' (O'Neill 2006), referring to a generalized cylinder. But I avoid this term here.

While 'pitch' is used often with circular helices to refer to the slope of the helix (e.g., Chouaieb *et al.* 2006), strictly speaking, pitch is the distance between adjacent threads or strands. Lead, on the other hand, is the axial progression per one full revolution of the helical structure, which is the quantity of interest in this study. Lead and pitch are the same for single-thread helices, but not for double or triple helices, such as in double- and multi-start screws and various helical structures in biology.

The slope of the helix, $\tan\lambda$, can be measured by the lead angle, as in this study, by the 'helix slope' itself (e.g., De Renzi & Mayoral 2024; also 'rise', Hauser *et al.* 2017), or by the 'helix angle', relative to the fixed axis (the complementary angle to the lead angle; Nutbourne & Martin 1988). The latter was referred to as 'inclination angle' by Moseley (1842), in his work on conchyliometry. However, more recently, inclination angle is used to describe the orientation of the aperture itself relative to the coiling axis (Schindel 1990; Vermeij 1993; Noshita *et al.* 2012), so I avoid this term here.

Finally, the quantity $u = \sqrt{\kappa^2 + \tau^2}$, which is the norm of the Darboux vector, where κ is curvature and τ is torsion, does not have a standard name. Nutbourne & Martin (1988) refer to it as 'compound curvature', and Güzelkardeşler & Şahiner (2024) call it 'first alternative curvatrue'. Other appropriate terms may be 'torque' or 'twirl(ing)' (Illert 1987), and 'winding', 'writhe', or 'twist', in reference to circular helices (Chouaieb *et al.* 2006; Goriely 2017); but those usually involve additional meaning in terms of mechanical properties. It is also sometimes called angular rate, speed, or velocity, though time is only implicit here, and u measures

rotation angle per unit arclength, not time. By the same token, the use of the term ‘spin’ is rejected. In this study, I refer to the Darboux vector and its norm, as well as to $\mathbf{w}$ and w, simply as vectors and rates of coiling, as in the end, they describe direction and rate of rotation. While the greek letter ω is often used to denote the Darboux vector and $\sqrt{\kappa^2+\tau^2}$ (Nutbourne & Martin 1988), I avoid this notation, so not to confuse with true angular velocity in mechanics.

S2 Expressions for logarithmic conispirals

Eq.[1] of the main text, $\cot\alpha\sin\beta=\gamma$, has been derived and used enough times, so not to require any explanation (Moseley 1842; Thompson [1942] 1992; Raup & Graus 1972; Løvtrup & von Sydow 1974; Ekaratne & Crisp 1983; Illert 1983). From geometry of cones, it is easy to see that

$$\sin\lambda=\cos\alpha\cos\beta \tag{S1}$$

(Moseley 1842; up to differences in notation and definition of lead angle), the expression for spiral height dilation, q_z. These two equations can be combined to produce

$$\tan\lambda\tan\beta=\frac{\gamma}{\sqrt{1+\gamma^2}}. \tag{S2}$$

Values of γ for gastropods are typically below 0.2 (Thompson [1942] 1992; Cameron 1981; Fig. 3), corresponding to relatively slower expansion and shells that exhibit several complete whorls. For small values of γ, Eq.[S2] is approximated by Eq.[2] of the main text.

The expression for a conispiral shell’s height-to-arclength ratio, derived by Ekaratne & Crisp (1983), can be written as $(z+b)/s$ in this study, which translates to $q_z+q_b=\sin\lambda+q_b$. Alternatively, using the steps of their derivation and following the suture spiral on the outer surface of the shell, rather than the centerline spiral, $(z/W+2b)/s=(1/W)\sin\lambda+(2\rho a/s)=(1/W)\sin\lambda+\rho r/s=\sin\lambda(1/W+\rho\tan\beta)$ (where s, r, λ and β all refer now to the suture spiral, W is the whorl expansion rate [Eq.[S3] below], and using the relations $\rho=b/a$, $r=2a$, and $r=z\tan\beta=s\sin\lambda\tan\beta$). In any case, all these ratios are constants for self-similar logarithmic conispiral shells.

S3 Whorl-overlap condition for non-circular and displaced generating curves

Mathematical and computational shell modeling got a boost with the work of David Raup in the 1960s (Raup 1961; Raup & Michelson 1965; Raup 1966) that also kick-started theoretical morphology. Raup's model for gastropod shell coiling (Raup 1961, 1966; Raup & Michelson 1965) contains four parameters that are designed to be estimated from sagittal cross-sections of shells. His whorl expansion rate, W, is related to γ through

$$W = e^{2\pi\gamma}. \tag{S3}$$

His translation rate, T, is related to β by

$$T = \cot\beta. \tag{S4}$$

The *displacement* (Schindel 1990) parameter, D, measures relative distance of the aperture from the coiling axis, and is given by

$$D = \frac{r-a}{r+a}, \tag{S5}$$

where a is aperture size in the radial direction (i.e., half the aperture's width in the r-direction). The umbilicus (or columellar) radius, ξ, i.e., distance of innermost aperture margin to the coiling axis, and the aperture size, a, are then given by

$$\begin{aligned} a &= \left(\tfrac{1-D}{1+D}\right) r, \\ \xi &= r - a = \left(\tfrac{2D}{1+D}\right) r. \end{aligned} \tag{S6}$$

Raup's fourth parameter, S, broadly refers to the shape of the generating curve, and is never really defined in his formulation. In principle, it may be vector- or function-valued, e.g., $S = S(\varphi)$ (φ being some parameterization of the generating curve). It is, however, very often taken to be some ratio of major and minor axes of an ellipse — a natural extension of the circular generating curve (Raup 1966; Kohn & Riggs 1975; Newkirk & Doyle 1975; McNair *et al.* 1981; Ekaratne & Crisp 1983; Kemp & Bertness 1984; Ackerly 1992; Stone 1995; McGhee 1999; Clarke *et al.* 1999; Urdy *et al.* 2010; Larsson *et al.* 2020). Here, I follow Ekaratne & Crisp (1983) and define aperture size a, perpendicular to the coiling axis, and aperture size b, parallel to the axis, as illustrated in Fig. 1*F* of main text.

The centers of two successive whorls (separated by $\Delta\theta = 2\pi$) are at distances r and rW from the coiling axis. Their distances to the apex are $r\sqrt{1+T^2}$ and $rW\sqrt{1+T^2}$, respectively. Aperture sizes along the conical envelope of the centerline spiral, i.e., at angle β to the coiling axis, are given by the radii of the elliptic generating curves at that angle $\frac{\rho a}{\sqrt{\rho^2\sin^2\beta+\cos^2\beta}}$ and

$\frac{\rho a W}{\sqrt{\rho^2 \sin^2\beta + \cos^2\beta}}$ respectively, where $\rho = b/a$. The whorl overlap condition is therefore,

$$r(W-1)\sqrt{1+T^2} < \frac{a\rho(W+1)\sqrt{1+T^2}}{\sqrt{\rho^2+T^2}}. \tag{S7}$$

(recall that $T = \cot\beta$, and so $\sin^2\beta = \frac{1}{1+T^2}$ and $\cos^2\beta = \frac{T^2}{1+T^2}$). Substituting the expression for a from Eq.[S6], and further trivial manipulations give

$$T^2 < \rho^2 \left(\frac{\left(\frac{1-D}{1+D}\right)^2 (W+1)^2 - (W-1)^2}{(W-1)^2} \right), \tag{S8}$$

or

$$T^2 < \rho^2 \frac{4W + 4D^2W - 4DW^2 - 4D}{(1+D)^2(W-1)^2}. \tag{S9}$$

Substituting circular apertures ($\rho = 1$) in Eq.[S8] results in Rex & Boss's (1976) expression for the boundary between whorl-overlap and open coiling. For a circular aperture ($\rho = 1$) touching the coiling axis ($D = 0$), I obtain Raup's (1966) expression for the "univalve-bivalve" boundary, $T = \frac{2\sqrt{W}}{W-1}$, on the W-T face of his morphospace cube. Substituting $T = 0$ in Eq.[S7] gives the "univalve-bivalve" boundary on the W-D face, $D < 1/W$, which is Raup's (1966) whorl-overlap condition for planispiral shells.

In terms of γ and β, Eq.[S8] can be rewritten as

$$\cot^2\beta < \rho^2 \left(\left(\frac{1-D}{1+D}\right)^2 \coth^2(\pi\gamma) - 1 \right) = \rho^2 \left(\left(\frac{1-D}{1+D}\right)^2 \frac{1}{\sinh^2(\pi\gamma)} - \frac{4D}{(1+D)^2} \right) \tag{S10}$$

or

$$\tan\beta > \frac{1+D}{\rho} \frac{\sinh(\pi\gamma)}{\sqrt{(1-D)^2 - 4D\sinh^2(\pi\gamma)}}. \tag{S11}$$

For circular apertures ($a = b$; $\rho = 1$) and $D = 0$, this equation gives the expression of Raup's whorl-overlap boundary in terms of γ and β of this study, $\tan\beta = \sinh(\pi\gamma)$.

From Eq.[S10] one can get the condition for whorl-overlap in terms of $\sin\beta$,

$$\sin^2\beta > \frac{1}{\rho^2 \left(\frac{1-D}{1+D}\right)^2 \coth^2(\pi\gamma) + (1-\rho^2)}. \tag{S12}$$

For $D = 0$ this simplifies to

$$\sin^2\beta > \frac{\sinh^2(\pi\gamma)}{\sinh^2(\pi\gamma) + \rho^2}. \tag{S13}$$

For $D = 0$ and $\rho = 1$, the condition further reduces to $\sin\beta > \tanh\pi\gamma$, the expression arrived at by Clarke *et al.* (1999; after correcting their typo and accounting for difference in definition of apical semiangle).

Combining Eq.[S11] and Eq.[S2], I get the whorl-overlap boundary in terms of lead angle,

$$\tan\lambda < \frac{\rho}{1+D} \frac{\gamma\sqrt{(1-D)^2 - 4D\sinh^2(\pi\gamma)}}{\sqrt{1+\gamma^2}\sinh(\pi\gamma)}. \tag{S14}$$

Applying the small-γ approximation, the whorl overlap condition for lead angle becomes

$$\tan\lambda < \left(\frac{1-D}{1+D}\right)\frac{\rho}{\pi} + \mathcal{O}(\gamma^2), \tag{S15}$$

providing the corresponding fixed value of lead angle that matches the whorl overlap condition for particular aperture shape, ρ, and aperture displacement, D.

One should note that, from Eq.[S6], $\frac{1-D}{1+D}\rho = b/r$. Consequently, the whorl-overlap conditions for $\tan\beta$ and $\tan\lambda$ (Eqs.[S11] and [S14]) can be be rewritten using the ratio $b/r = q_b/q_r$, instead of $\rho = b/a$, giving $\tan\beta > \frac{q_r}{q_b}\pi\gamma + \mathcal{O}(\gamma^3)$ and $\tan\lambda < \frac{q_b}{q_r}\frac{1}{\pi} + \mathcal{O}(\gamma^2)$, respectively. But I conform here to much past literature by using D and ρ as the independent parameters (Raup 1966; Kohn & Riggs 1975; Ekaratne & Crisp 1983; Gerber 2017). Ultimately, the purpose of the shape parameter (be it $\rho = q_b/q_a$, or q_b/q_r) is to set the upper and lower curves for whorl-overlap and their corresponding fixed lead angles in Fig. 2. Similarly, if considering aperture height in the normal plane, b^* in Fig. 2*F*, rather than in the sagittal whorl-cross-section plane, such that $b = b^*/\cos\lambda$, the whorl overlap condition becomes a condition on $\sin\lambda$, rather than $\tan\lambda$, in Eqs.[S14] and [S15].

S4 Approximation errors

For the range of γ-values exhibited by most gastropods, $\gamma \leq 0.2$ (Thompson [1942] 1992; Cameron 1981), the error between the full and approximate versions of Eq.[S2] (Eq.[2] in the main text) is no more than 2%. This is derived from the ratio of the right-hand-sides of Eq.[2] and Eq.[S2], $\sqrt{1+\gamma^2}$, which clearly increases with γ, and is 1 for $\gamma = 0$ and 1.0198 for $\gamma = 0.2$.

S5 Differential geometric parameterization

The typical approach in differential geometry is to follow the Frenet frame, attached to a space curve; though other local (moving) frames are possible (Moulton *et al.* 2012; Moulton & Goriely 2014; Uzunoğlu *et al.* 2016; Goriely 2017; Güzelkardeşler & Şahiner 2024 ; see below). The Frenet frame is composed of the tangent, principal normal, and binormal unit vectors of the space curve, $\hat{\mathbf{t}}$, $\hat{\mathbf{n}}$, and $\hat{\mathbf{b}}$, respectively, parameterized by arclength, s, along the curve. The frame changes along the curve according to the Frenet-Serret differential equations,

$$\begin{aligned}
\hat{\mathbf{t}}' &= \frac{\mathrm{d}\hat{\mathbf{t}}}{\mathrm{d}s} = \mathbf{u}\times\hat{\mathbf{t}} = \kappa\hat{\mathbf{n}} \\
\hat{\mathbf{n}}' &= \mathbf{u}\times\hat{\mathbf{n}} = \tau\hat{\mathbf{b}} - \kappa\hat{\mathbf{t}} \\
\hat{\mathbf{b}}' &= \mathbf{u}\times\hat{\mathbf{b}} = -\tau\hat{\mathbf{n}},
\end{aligned} \tag{S16}$$

where $\times$ is vector cross-product in 3D Euclidean space, $\mathbf{u}$ is the Darboux vector,

$$\mathbf{u} = u\hat{\mathbf{u}} = \tau\hat{\mathbf{t}} + \kappa\hat{\mathbf{b}}, \tag{S17}$$

u is the vector's magnitude (i.e., local coiling; or the compound curvature of Nutbourne & Martin 1988; see §S1), $\kappa = u\cos\lambda$ is curvature, and $\tau = u\sin\lambda$ is torsion. The Darboux vector, thus, describes the instantaneous rotation of the Frenet moving-frame, with respect to arclength (rather than time). For generalized helices ($\tau/\kappa = \tan\lambda = \text{const}$), including conical helices, the direction of the Darboux vector is fixed, $\hat{\mathbf{u}}' = 0$, though coiling rate, u, itself can change (e.g., for conical helices $u \propto 1/s$). In other words, for generalized helices $\mathbf{u}' = u'\hat{\mathbf{u}}$, and the direction $\hat{\mathbf{u}}$ determines the fixed coiling axis of the helix.

If lead angle changes with arclength, the space curve is no longer a generalized helix, and the direction of $\mathbf{u}$ changes along the curve, $\hat{\mathbf{u}}' \neq 0$ and $\mathbf{u}' = u'\hat{\mathbf{u}} + u\hat{\mathbf{u}}'$. Because $\hat{\mathbf{u}}$ is a unit vector, its derivative can be written as a cross-product with some instantaneous rotation vector, $\mathbf{w}$, such that $\hat{\mathbf{u}}' = \mathbf{w} \times \hat{\mathbf{u}}$. For generalized helices $\mathbf{w} \equiv \mathbf{u}$, and so $\hat{\mathbf{u}}' = \mathbf{u} \times \hat{\mathbf{u}} = u\hat{\mathbf{u}} \times \hat{\mathbf{u}} \equiv 0$. In the general case, we write $\mathbf{w} = w_1\hat{\mathbf{t}} + w_2\hat{\mathbf{n}} + w_3\hat{\mathbf{b}}$, and attempt to find the w_i from Eqs.[S16] and [S17].

First, note that from Eq.[S17] $\hat{\mathbf{u}} = \hat{\mathbf{t}}\sin\lambda + \hat{\mathbf{b}}\cos\lambda$, and therefore by applying the Frenet-Serret relations (Eq.[S16]), $\hat{\mathbf{u}}' = (\hat{\mathbf{t}}\cos\lambda - \hat{\mathbf{b}}\sin\lambda)\lambda'$. Expanding the rotation vector, $\mathbf{w} \times \hat{\mathbf{u}} = (-w_2\hat{\mathbf{b}} + w_3\hat{\mathbf{n}})\sin\lambda + (-w_1\hat{\mathbf{n}} + w_2\hat{\mathbf{t}})\cos\lambda$. Equating the two expressions per component, one obtains $w_2 = \lambda'$, and $w_3 = w_1\cot\lambda$, while w_1 still remains unknown. We can already guess, based on $\mathbf{w} = \mathbf{u}$ for generalized helices, that $w_1 = u\sin\lambda = \tau$ and $w_3 = u\cos\lambda = \kappa$. That is corroborated by noting that the Darboux vector does not have a $\hat{\mathbf{n}}$-component, i.e., $\hat{\mathbf{u}}$ and $\hat{\mathbf{n}}$ are always perpendicular to each other. Consequently, we can construct the alternative orthonormal moving-frame of Uzunoğlu *et al.* (2016) and Güzelkardeşler & Şahiner (2024), composed of $\hat{\mathbf{u}}$, $\hat{\mathbf{n}}$, and $\hat{\mathbf{u}} \times \hat{\mathbf{n}}$. The rotation vector of this frame is $\mathbf{w}$, resulting in the relation $\hat{\mathbf{n}}' = \mathbf{w} \times \hat{\mathbf{n}} = w_1\hat{\mathbf{b}} - w_3\hat{\mathbf{t}}$. But from the Frenet-Serret equations (Eq.[S16]) we know that $\hat{\mathbf{n}}' = \tau\hat{\mathbf{b}} - \kappa\hat{\mathbf{t}}$, and so $w_1 = \tau$ and $w_3 = \kappa$, or in vector form,

$$\begin{aligned} \mathbf{w} &= w\hat{\mathbf{w}} = \mathbf{u} + \lambda'\hat{\mathbf{n}} = u\hat{\mathbf{u}} + \lambda'\hat{\mathbf{n}}, \\ w &= \sqrt{u^2 + (\lambda')^2}, \end{aligned} \tag{S18}$$

the vector and rate of total coiling, respectively. Comparing again to Uzunoğlu *et al.* (2016) and Güzelkardeşler & Şahiner (2024), u is their 'first alternative curvature', and λ' their 'second alternative curvature'. Generalized helices are obtained when the second alternative curvature vanishes, $\lambda' = 0$ (Güzelkardeşler & Şahiner 2024). Substituting the identity $\tan\lambda = \kappa/\tau$ into their expression for the second alternative curvature, $\frac{\kappa^2}{\kappa^2+\tau^2}(\kappa/\tau)'$, clearly results in $\cos^2\lambda\,\mathrm{d}\tan\lambda/\mathrm{d}s$, which reduces to simply $\mathrm{d}\lambda/\mathrm{d}s \equiv \lambda'$. Namely, the second alternative curvature is simply the rate of change in lead angle, which I refer to as rate of *coiling precession*.

For generalized helices ($\lambda = \text{const}$), $\mathbf{w} = \mathbf{u}$, $\hat{\mathbf{u}}' = \mathbf{w} \times \hat{\mathbf{u}} = -\lambda'(\hat{\mathbf{u}} \times \hat{\mathbf{n}}) = 0$, and there is a fixed

S191 coiling axis, coinciding with a fixed Darboux vector. However, in general, the vector $\mathbf{w}$ defines a
S192 precession of the Darboux vector (recall that $\mathbf{u}$ is the instantaneous rotation of the Frenet
S193 frame), and is itself not fixed. In some special cases, when $u = \text{const}$ and $\mathbf{w}$ fixed, one can
S194 obtain the 'modulated curves' of Nutbourne & Martin (1988), better known as 'curves of
S195 constant precession' (Scofield 1995).

S196 A slant helix is, similarly, a class of precession curves that includes the generalized helix
S197 and the curves of constant precession as special cases. The defining feature of a slant helix
S198 is a constant angle between the principal normal of the curve, $\hat{\mathbf{n}}$, and some fixed direction in
S199 space. In generalized helices, that angle is 90°. Izumiya & Takeuchi's (2004) necessary and
S200 sufficient condition for a slant helix translates, in the notation of this study, to the
S201 proportionality relationship $\lambda' = \sigma u$. In other words, second alternative curvature is
S202 proportional to first alternative curvature, with a proportionality constant σ. The total coiling
S203 vector becomes $\mathbf{w} = w\hat{\mathbf{w}} = u(\hat{\mathbf{u}} + \sigma\hat{\mathbf{n}})$, and $\hat{\mathbf{w}}$ defines a fixed axis of rotation (or coiling), though
S204 coiling rate, $w = u\sqrt{1+\sigma^2}$, around the fixed axis generally varies. That can be verified by
S205 $\sqrt{1+\sigma^2}\hat{\mathbf{w}}' = (\hat{\mathbf{u}} + \sigma\hat{\mathbf{n}})' = \mathbf{w} \times \hat{\mathbf{u}} + \sigma\mathbf{w} \times \hat{\mathbf{n}} = (\sigma u\hat{\mathbf{n}}) \times \hat{\mathbf{u}} + \sigma(u\hat{\mathbf{u}} \times \hat{\mathbf{n}}) = 0$.

S206 Finally, note that the lead angle, λ, is defined in the $\hat{\mathbf{t}}$-$\hat{\mathbf{b}}$ plane, the *rectifying plane* of the space
S207 curve. For generalized helices, this plane is parallel to the coiling axis, i.e. z-axis, and lead
S208 angle therefore is the angle between $\hat{\mathbf{t}}$ and the r-θ (or x-y) plane, perpendicular to the coiling
S209 axis; or, alternatively, the z-component of $\hat{\mathbf{t}}$ is $\sin\lambda$. That is no longer the case for slant helices.
S210 The rectifying plane now revolves around the coiling axis at a fixed tilt, given by $\arctan(\sigma)$. Lead
S211 angle is still defined in the rectifying plane, and therefore the tangent vector, $\hat{\mathbf{t}}$, which is also the
S212 unit velocity vector of the space curve w.r.t to arclength, is given in Cartesian coordinates by

S213
$$\hat{\mathbf{t}} = (-\cos\lambda\sin\theta + c\sin\lambda\cos\theta)\hat{\mathbf{x}} + (\cos\lambda\cos\theta + c\sin\lambda\sin\theta)\hat{\mathbf{y}} + \sqrt{1-c^2}\sin\lambda\hat{\mathbf{z}},$$
$$\text{where } c = \frac{\sigma}{\sqrt{1+\sigma^2}} = \text{const}, \tag{S19}$$

S214 and $\lambda = \lambda(s)$, $\theta = \theta(s)$. The rotation of $\hat{\mathbf{t}}$ is still given by the Frenet-Serret relations (Eq.[S16]),
S215 which translates in the case of slant helices to $\hat{\mathbf{t}}' = (\mathbf{w} - \lambda'\hat{\mathbf{n}}) \times \hat{\mathbf{t}} = \mathbf{w} \times \hat{\mathbf{t}} - \lambda'\hat{\mathbf{n}} \times \hat{\mathbf{t}}$. In other words,
S216 as expected, a combination of rotation around the axis, $\hat{\mathbf{w}}$, and rotation within the $\hat{\mathbf{t}}$-$\hat{\mathbf{b}}$ plane at
S217 an angular rate λ', as lead angle increases (with the axis of the latter rotation being $-\hat{\mathbf{n}}$; again,
S218 as expected according to the definition of lead angle).

S6 Logarithmic slant helix

For the logarithmic slant helix, $u = \tilde{u}/s$. Consequently, $\lambda' = \sigma\tilde{u}/s$ and $w = \tilde{w}/s$, where $\tilde{w} = \tilde{u}\sqrt{1+\sigma^2}$. Given that $\mathrm{d}\theta/\mathrm{d}s = w$, it is straightforward to get relations comparable to conical helices for revolution angle and arclength, $\theta = \tilde{w}\ln(s/s_0)$ and $s = s_0 e^{\gamma\theta}$, where $\gamma = 1/\tilde{w}$ (in this section, $\gamma \equiv \gamma_s$). Given $\lambda' = \mathrm{d}\lambda/\mathrm{d}s = \sigma u = c\,w = c\,\mathrm{d}\theta/\mathrm{d}s$ (c as in Eq.[S19]), lead angle increases linearly with revolution angle according to $\lambda = \lambda_0 + c\theta$. From these expressions one can obtain the position vector of the logarithmic slant helix, $x(\theta)\hat{\mathbf{x}} + y(\theta)\hat{\mathbf{y}} + z(\theta)\hat{\mathbf{z}}$, by integrating $(\mathrm{d}s/\mathrm{d}\theta)\hat{\mathbf{t}}(s)$ w.r.t to θ, given Eq.[S19] for $\hat{\mathbf{t}}(s)$,

$$z(\theta) = C_z + \sqrt{1-c^2}\,s_0 e^{\gamma\theta}\left(\frac{\gamma^2\sin(c\theta+\lambda_0) - c\gamma\cos(c\theta+\lambda_0)}{c^2+\gamma^2}\right), \tag{S20}$$

$$\begin{aligned} x(\theta) = C_x + \frac{\gamma s_0 e^{\gamma\theta}}{c^4 + 2c^2\gamma^2 - 2c^2 + \gamma^4 + 2\gamma^2 + 1}(&-c^4\cos\lambda\cos\theta + c^3\gamma\sin\lambda\cos\theta - 2c^3\sin\lambda\sin\theta \\ &- c^2\gamma^2\cos\lambda\cos\theta - 3c^2\gamma\sin\theta\cos\lambda + c\gamma^3\sin\lambda\cos\theta + 3c\gamma\sin\lambda\cos\theta + 2c\sin\lambda\sin\theta \\ &- \gamma^3\sin\theta\cos\lambda + \gamma^2\cos\lambda\cos\theta - \gamma\sin\theta\cos\lambda + \cos\lambda\cos\theta), \end{aligned} \tag{S21}$$

$$\begin{aligned} y(\theta) = C_y + \frac{\gamma s_0 e^{\gamma\theta}}{c^4 + 2c^2\gamma^2 - 2c^2 + \gamma^4 + 2\gamma^2 + 1}(&-c^4\sin\theta\cos\lambda + c^3\gamma\sin\lambda\sin\theta + 2c^3\sin\lambda\cos\theta \\ &- c^2\gamma^2\sin\theta\cos\lambda + 3c^2\gamma\cos\lambda\cos\theta + c\gamma^3\sin\lambda\sin\theta + 3c\gamma\sin\lambda\sin\theta \\ &- 2c\sin\lambda\cos\theta + \gamma^3\cos\lambda\cos\theta + \gamma^2\sin\theta\cos\lambda + \gamma\cos\lambda\cos\theta + \sin\theta\cos\lambda), \end{aligned} \tag{S22}$$

where C_z, C_x, C_y are determined from initial conditions, and $\lambda = \lambda(\theta) = \lambda_0 + c\theta$. These expressions for $x(\theta)$, $y(\theta)$ and $z(\theta)$, can be used in computer graphics to simulate shells that follow a logarithmic slant helix centerline.

S7 Web application

For this study, I have also written a `WebGL` application to help with creating images of shells, as in Fig. 1. Snapshot of the code, coinciding with the publication of this report, is available at https://doi.org/10.5281/zenodo.19895626.

- WebApp options and parameters for Fig. 1*A*–*C* are Shell unchecked, Centerline spiral checked, Generating curve unchecked, and either Planispiral (panel A) or Circular helix (panel C) additionally selected. Pitch angle 69°, Roll angle 200°, $\lambda_0 = 0.22$, $\tilde{w} = 11.43$ ($\gamma = 0.0875$), $\sigma = 0$.
- Parameters for Fig. 1*E* are Pitch angle 270, Roll angle 64, Shell and Multispirals checked, Generating curve unchecked. $\lambda_0 = 0.39$, $\tilde{w} = 9.38$ ($\gamma = 0.107$), $\sigma = 0$.

- For Fig. 1*F*, Pitch angle 70, Roll angle 257. Shell, Centerline spiral, and Generating curve checked. $\lambda_0 = 0.22$, $\tilde{w} = 11.43$ ($\gamma = 0.0875$), $\sigma = 0$.

- Parameters for Fig. 1*G* are Pitch angle 69, Roll angle 300, Shell deselected, Centerline spiral checked, Generating curve unchecked, $\lambda_0 = 0$, $\tilde{w} = 11.43$ ($\gamma = 0.0875$), $\sigma = 0.013$.

- Parameters for Fig. 1*H* are Pitch angle 69, Roll angle 36, Shell deselected, Centerline spiral checked, Generating curve unchecked, $\lambda_0 = 0$, $\tilde{w} = 18.99$ ($\gamma = 0.0527$), $\sigma = 0.01$.

- For Fig. 1*I*, Pitch angle 62, Roll angle 152, Shell, Centerline spiral, and Generating curve checked, $\lambda_0 = 0$, $\tilde{w} = 5.85$ ($\gamma = 0.171$), $\sigma = 0.21$.

S8 Supplementary references

Ackerly SC (1992). The structure of ontogenetic variation in the shell of *Pecten*. *Palaeontology* 35: 847–867.

Cameron RAD (1981). Functional aspects of shell geometry in some british land snails. *Biol J Linn Soc* 16: 157–167. https://doi.org/10.1111/j.1095-8312.1981.tb01648.x.

Chouaieb N, Goriely A, Maddocks JH (2006). Helices. *Proc Natl Acad Sci USA* 103: 9398–9403. https://doi.org/10.1073/pnas.0508370103.

Clarke RK, Grahame J, Mill PJ (1999). Variation and constraint in the shells of two sibling species of intertidal rough periwinkles (Gastropoda: *Littorina* spp.). *J Zool* 247: 145–154. 10.1111/j.1469-7998.1999.tb00978.x.

De Renzi M, Mayoral E (2024). Understanding behaviour through theoretical morphology: the case of helical-shaped burrows. *J Iber Geol* 50: 549–566. https://doi.org/10.1007/s41513-024-00249-7.

Ekaratne SUK, Crisp DJ (1983). A geometric analysis of growth in gastropod shells, with particular reference to turbinate forms. *Journal of Marine Biology Association UK* 63: 777–797. 10.1017/S0025315400071216.

Gerber S (2017). The geometry of morphospaces: lessons from the classic Raup shell coiling model. *Biol Rev* 92: 1142–1155. https://doi.org/10.1111/brv.12276.

Goriely A (2017). *The Mathematics and Mechanics of Biological Growth*. Springer. https://doi.org/10.1007/978-0-387-87710-5.

Güzelkardeşler G, Şahiner B (2024). An alternative approach to find the position vector of a general helix. *Celal Bayar University Journal of Science* 20: 54–60. 10.18466/cbayarfbe.1479066.

Hauser K, He Y, Garcia-Diaz M, Simmerling C, Coutsias E (2017). Characterization of biomolecular

helices and their complementarity using geometric analysis. *Journal of Chemical Information and Modeling* 57: 864–874. https://doi.org/10.1021/acs.jcim.6b00721.

Illert C (1983). The mathematics of gnomonic seashells. *Math Biosci* 63: 21–56. 10.1016/0025-5564(83)90049-4.

Illert C (1987). Formulation and solution of the classical seashell problem. I. - Seashell geometry. *Il Nuovo Cimento D* 9: 791–814. 10.1007/BF02453750.

Izumiya S, Takeuchi N (2004). New special curves and developable surfaces. *Turkish Journal of Mathematics* 28: 153–164. 10.14943/83700.

Kemp P, Bertness MD (1984). Snail shape and growth rates: evidence for plastic shell allometry in *Littorina littorea*. *Proc Natl Acad Sci USA* 81: 811–813. https://doi.org/10.1073/pnas.81.3.811.

Kohn AJ, Riggs AC (1975). Morphometry of the *Conus* shell. *Syst Zool* 24: 346–359. 10.1093/sysbio/24.3.346.

Larsson J, Westram AM, Bengmark S, Lundh T, Butlin RK, Butlin RK (2020). A developmentally descriptive method for quantifying shape in gastropod shells. *J R Soc Interface* 17. http://dx.doi.org/10.1098/rsif.2019.0721.

Løvtrup S, von Sydow B (1974). D'Arcy Thompson's theorem and the shape of the molluscan shell. *Bull Math Biol* 36: 567–575. 10.1016/S0092-8240(74)80051-0.

McGhee GR (1999). *Theoretical Morphology : The Concept and Its Applications*. Perspectives in Earth History and Paleobiology. Columbia University Press, New York.

McNair C, Kier W, LaCroix P, Linsley R (1981). The functional significance of aperture form in gastropods. *Lethaia* 14: 63–70. 10.1111/j.1502-3931.1981.tb01076.x.

Moseley H (1842). On conchyliometry. *Lond Edinb Dubl Phil Mag* 21: 300–305. https://doi.org/10.1080/14786444208621551.

Moulton D, Goriely A, Chirat R (2012). Mechanical growth and morphogenesis of seashells. *J Theor Biol* 311: 69–79. https://doi.org/10.1016/j.jtbi.2012.07.009.

Moulton DE, Goriely A (2014). Surface growth kinematics via local curve evolution. *J Math Biol* 68: 81–108. 10.1007/s00285-012-0625-7.

Newkirk GF, Doyle RW (1975). Genetic analysis of shell-shape variation in *Littorina saxatilis* on an environmental cline. *Mar Biol* 30: 227–237. 10.1007/BF00390745.

Noshita K, Asami T, Ubukata T (2012). Functional constraints on coiling geometry and aperture inclination in gastropods. *Paleobiology* 38: 322–334. 10.1666/10060.1.

S302 Nutbourne AW, Martin RR (1988). *Differential geometry applied to curve and surface design:*
S303 *Foundations.* Ellis Horwood, Chichester, England.

S304 O'Neill B (2006). *Elementary Differential Geometry.* Revised 2nd edn. Academic Press.

S305 Raup DM (1961). The geometry of coiling in gastropods. *Proc Natl Acad Sci USA* 47: 602–609.
S306 https://doi.org/10.1073/pnas.47.4.602.

S307 Raup DM (1966). Geometric analysis of shell coiling: general problems. *J Paleontol* 40: 1178–1190.

S308 Raup DM, Graus RR (1972). General equations for volume and surface area of a logarithmically coiled
S309 shell. *Mathematical Geology* 4: 307–316. 10.1007/BF02114092.

S310 Raup DM, Michelson A (1965). Theoretical morphology of the coiled shell. *Science* 147: 1294–1295.
S311 10.1126/science.147.3663.1294.

S312 Rex MA, Boss KJ (1976). Open coiling in recent gastropods. *Malacologia* 15: 289–297.

S313 Schindel DE (1990). Unoccupied morphospace and the coiled geometry of gastropods: architectural
S314 constraint or geometric covariation? In *Causes of Evolution: a paleontological perspective* (edited by
S315 Ross R, Allmon W), pp. 270–304. University of Chicago Press, Chicago.

S316 Scofield PD (1995). Curves of constant precession. *The American Mathematical Monthly* 102: 531–537.
S317 https://doi.org/10.1080/00029890.1995.12004613.

S318 Stone JR (1995). CerioShell: a computer program designed to simulate variation in shell form.
S319 *Paleobiology* 21: 509–519. 10.1017/S0094837300013518.

S320 Thompson DW ([1942] 1992). *On Growth and Form: The Complete Revised Edition.* Dover, New York.

S321 Urdy S, Goudemand N, Bucher H, Chirat R (2010). Allometries and the morphogenesis of the
S322 molluscan shell: a quantitative and theoretical model. *J Exp Zool* 314B: 280–302.
S323 10.1002/jez.b.21337.

S324 Uzunoğlu B, Gök I, Yaylı Y (2016). A new approach on curves of constant precession. *Applied*
S325 *Mathematics and Computation* 275: 317–323. https://doi.org/10.1016/j.amc.2015.11.083.

S326 Vermeij GJ (1993). *A Natural History of Shells.* Princeton University Press, Princeton, Oxford.